J Membrane Biol (2010) 235:73–87
DOI 10.1007/s00232-010-9257-2

Characterization of the Rapidly Activating Delayed Rectifier Potassium Current, I_{Kr}, in HL-1 Mouse Atrial Myocytes

Futoshi Toyoda · Wei-Guang Ding · Dimitar P. Zankov · Mariko Omatsu-Kanbe · Takahiro Isono · Minoru Horie · Hiroshi Matsuura

Received: 29 November 2009 / Accepted: 29 April 2010 / Published online: 19 May 2010

Abstract HL-1 is the adult murine cardiac cell line that can be passaged repeatedly in vitro without losing differentiated phenotype. The present study was designed to characterize the rapidly activating delayed rectifier potassium current, I_{Kr}, endogenously expressed in HL-1 cells using the whole-cell patch-clamp technique. In the presence of nisoldipine, depolarizing voltage steps applied from a holding potential of −50 mV evoked the time-dependent outward current, followed by slowly decaying outward tail current upon return to the holding potential. The amplitude of the current increased with depolarizations up to 0 mV but then progressively decreased with further depolarizations. The time-dependent outward current as well as the tail current were highly sensitive to block by E-4031 and dofetilide (IC_{50} of 21.1 and 15.1 nM, respectively) and almost totally abolished by micromolar concentrations of each drug, suggesting that most of the outward current in HL-1 cells was attributable to I_{Kr}. The magnitude of I_{Kr} available from HL-1 cells (18.1 ± 1.5 pA pF^{-1}) was sufficient for reliable measurements of various gating parameters. RT-PCR and Western blot analysis revealed the expression of alternatively spliced forms of mouse *ether-a-go-go*-related genes (mERG1), the full-length mERG1a and the N-terminally truncated mERG1b isoforms. Knockdown of mERG1 transcripts with small interfering RNA (siRNA) dramatically reduced I_{Kr} amplitude, confirming the molecular link of mERG1 and I_{Kr} in HL-1 cells. These findings demonstrate that HL-1 cells possess I_{Kr} with properties comparable to those in native cardiac I_{Kr} and provide an experimental model suitable for studies of I_{Kr} channels.

Keywords Cardiac cell line · Potassium current · Potassium channel · Patch-clamp · HL-1 cell · siRNA

F. Toyoda (✉) · W.-G. Ding · D. P. Zankov · M. Omatsu-Kanbe · H. Matsuura
Department of Physiology, Shiga University of Medical Science, Otsu, Shiga 520-2192, Japan
e-mail: toyoda@belle.shiga-med.ac.jp

D. P. Zankov · M. Horie
Department of Cardiovascular and Respiratory Medicine, Shiga University of Medical Science, Otsu, Shiga 520-2192, Japan

T. Isono
Central Research Laboratory, Shiga University of Medical Science, Otsu, Shiga 520-2192, Japan

Introduction

Cardiac delayed rectifier potassium current (I_K) is responsible for action potential repolarization and pacemaker activity and consists of multiple components with distinct time and voltage dependence and pharmacological properties. I_{Kr} is the rapidly activating, inwardly rectifying component of I_K, which can be isolated as a fraction specifically blocked by the class III antiarrhythmic methanesulfonanilide agents such as E-4031 and dofetilide (Sanguinetti and Jurkiewicz 1990). It is now well known that I_{Kr} is conducted by ERG1 (*ether-a-go-go*-related gene) potassium channels (Sanguinetti et al. 1995; Trudeau et al. 1995). Mutations in the human ERG1 (HERG) channel gene underlie the inherited long QT syndrome, a disorder of cardiac repolarization that predisposes affected individuals to life-threatening arrhythmias (Curran et al. 1995). In addition, I_{Kr} is sensitive to block by a diverse range of therapeutic agents (e.g., antihistamines, gastrointestinal prokinetic agents, psychoactive substances), and these adverse drug effects can induce acquired long QT syndrome (Roden et al. 1996).

Taking advantage of molecular biological technology, functional analysis of reconstituted HERG channels in a heterologous expression system has provided information on the gating mechanisms, modulation and drug block of I_{Kr} channels. Nevertheless, current recordings from native channels are still important because several differences between native I_{Kr} and reconstituted HERG current have been revealed (Sanguinetti et al. 1995; Weerapura et al. 2002), possibly due to inadequate composition of channel proteins or lack of cardiac-specific environments in the heterologous expression system. AT-1 cells, a cardiac cell line derived from atrial tumor of adult transgenic mice expressing the simian virus 40 (SV40) large T-antigen targeted to atrial cardiomyocytes via the atrial natriuretic factor (ANF) promoter (Field 1988), have been often employed as a suitable source of native I_{Kr} channels (Liu et al. 1994; Yang and Roden 1996; Yang et al. 1994, 1995, 1997). Membrane current recorded from these cells displays phenotypical characteristics of cardiac I_{Kr} with minimal contamination of other time-dependent outward currents. Maintenance of AT-1 cells, however, is complicated and labored because it is impossible to passage these cells serially in vitro. They are maintained by serial propagation as a subcutaneous tumor in syngeneic mice and have to be used as primary cells (Delcarpio et al. 1991).

The HL-1 cell line was derived from subsequent development of AT-1 cells (Claycomb et al. 1998). Different from any other cardiac cell lines currently available, HL-1 cells can be repeatedly passaged in culture while maintaining a differentiated cardiac phenotype. They express many cardiac-specific proteins such as α-myosin heavy chain, ANF, α-cardiac actin and connexin 43 (Claycomb et al. 1998). Furthermore, several functional receptors, such as α_1-adrenergic and δ-opioid receptors, and intracellular signaling proteins required for phosphatidylinositol hydrolysis and the cyclic AMP synthesis pathway have been demonstrated in HL-1 cells (McWhinney et al. 2000; Neilan et al. 2000; Sartiani et al. 2002). Recent patch-clamp studies have revealed the existence of several cardiac membrane currents, including I_{Kr} as well as the hyperpolarization-activated nonselective cation current (I_f) and the L- and T-type Ca^{2+} currents ($I_{Ca,L}$ and $I_{Ca,T}$) (Claycomb et al. 1998; Sartiani et al. 2002; Xia et al. 2004; Zankov et al. 2009). Thus, HL-1 cells may be used as a model of cardiac cells for studying many features of ion channels in a cardiac-specific environment (White et al. 2004).

The present study characterizes I_{Kr} channels endogenously expressed in HL-1 cells. Whole-cell patch-clamp experiments demonstrate that I_{Kr}, defined as the E-4031-sensitive current, can be elicited in almost all cells with current magnitude of 0.1–1.5 nA suitable for high-quality recording, which allows us to analyze biophysical and pharmacological features extensively and reliably. In addition, alternatively spliced forms of mouse ERG1 (mERG1) are identified in HL-1 cells, and our RNA interference (RNAi) experiments suggest that these ERG1 isoforms indeed underlie I_{Kr}. Data obtained here will be helpful for future applications of HL-1 cells as a unique model to study cardiac I_{Kr} channels.

Methods

Culture of HL-1 Cells

The HL-1 cell culture (passage 36) was a kind gift from Dr. Claycomb (Louisiana State University Health Science Center, New Orleans, LA) who first established the cell line. Care of the HL-1 cells was described previously (Claycomb et al. 1998). Claycomb medium (JRH Bioscience, Lenexa, KS; catalog 51800), a commercially available medium specifically designed for the growth of HL-1 cells, was purchased. Before use, the Claycomb medium was supplemented with 10% fetal bovine serum (JRH Bioscience), 2 mM L-glutamine (Invitrogen, Carlsbad, CA), 0.1 mM norepinephrine (Sigma, St. Louis, MO) and penicillin–streptomycin (Nakalai Tesque, Kyoto, Japan). The supplemented Claycomb medium was prepared every 2 weeks and kept in the dark by covering the medium bottle with aluminum foil because it is highly light-sensitive. Cells were plated on T25 flasks (Techno Plastic Products, Trasadingen, Switzerland; 90025) precoated overnight with 0.00125% fibronectin (Sigma, F1141) in 0.02% gelatin (Difco, Detroit, MI; 0143-17-9) and maintained in supplemented Claycomb medium at 37°C in humidified 5% CO_2 and 95% air. The culture medium was changed daily. After full confluence, cells were dissociated by 0.05% trypsin/EDTA (Invitrogen). Isolated cells were then suspended in Claycomb medium supplemented with 5% fetal bovine serum and antibiotics, and the cell suspension was used for the patch-clamp experiments or split into new flasks for subsequent culturing.

Reverse Transcription-Polymerase Chain Reaction Amplification

HL-1 cells culture (passage 40) and atrial tissue dissected from adult mice were used for mRNA purification. Total RNA from each sample was extracted by the acid guanidium thiocyanate chlorofrom method (Chomczynski and Sacchi 1987). cDNA was synthesized from 5 μg of total RNA with 20 units of RAV-2 reverse transcriptase (Takara, Otsu, Japan) using random primers. PCR for mouse ERG1 isoforms (mERG1a, mERG1a′ and mERG1b) was

performed using the following primer sets reported previously (Clark et al. 2004) (from 5 to 3): ACA CCT TCC TCG ACA CCA TC (sense; position 621–641, accession AF012870) and GCA TCA GGG TTA AGG CTC TG (antisense; position 1405–1424, accession AF012871) for mERG1a, ACC ACT GGC ATA GGA CCA AG (sense; position 839–858, accession AF012870) and the same antisense as for mERG1a for mERG1a′, ATG GCG ATT CCA GCC GGG AA (sense; position 3952–3971, accession AF012871) and GAT GCC ATT GGT GTA GGA CC (antisense; position 8239–8258, accession AF012871) for mERG1b. The reaction included 0.4 µl of cDNA, 2.5 units of KOD dash polymerase (Toyobo, Osaka, Japan), 1 mM KCl, 6 mM $(NH_4)_2SO_4$, 0.1% Triton X-100, 10 µg ml^{-1} BSA, 0.2 mM each of deoxynucleotide triphosphate and 4 pmol primers in 20 ml of 120 mM Tris–HCl buffer (pH 8.0). Amplification was conducted in a thermal cycler using 30 cycles consisting of denaturation at 98°C for 2 s, annealing at 55°C for 2 s and elongation at 72°C for 60 s. PCR products were identified in an ethidium bromide-stained 1.5% agarose gel by electrophoresis.

Western Blotting

HL-1 cells (passages 45–47) were washed with cold phosphate-buffered saline and resuspended in lysis buffer (50 mM Tris–HCl, 5 mM EDTA, 150 mM NaCl, 1% Triton X-100, pH 7.4) supplemented with a mix of protease inhibitors (Complete Mini; Roche, Mannheim, Germany). Cell lysate was centrifuged at 15,000 rpm for 5 min. Total protein was measured using the DC protein assay (Bio-Rad, Richmond, CA). For Western blot assay, 100 µg of total proteins were dissolved in 2 × SDS sample buffer (4% sodium dodecyl sulfate, 125 mM Tris–HCl, 12% 2-mercaptoethanol, 20% glycerol, 0.005% bromophenol blue, pH 6.8) and then sonicated and boiled for 5 min. Samples were resolved on 7.5% SuperSep gel (Wako, Osaka, Japan) and electrotransferred onto a polyvinylidene difluoride (PVDF) membrane (Bio-Rad). The membrane was blocked in Tris-buffered saline (TBS; 10 mM Tris–HCl, 100 mM NaCl, pH 7.5) containing 0.1% Tween-20 and 10% nonfat dry milk for 1.5 h at room temperature and then incubated overnight at 4°C with a rabbit polyclonal anti-ERG1 antibody (Chemicon, Temecula, CA; AB5222) directed against the C terminus (amino acid residues 1121–1137, accession O08962) of rat ERG1, at a dilution 1:200. After washing with TBS-Tween 0.1%, the membrane was incubated with a horseradish peroxidase-conjugated secondary anitibody (Jackson ImmunoResearch, West Grove, PA; 1:5,000) for 1 h at room temperature. Signals were detected using an enhanced chemiluminescence system.

RNAi

Two Stealth small interfering RNA (siRNA) duplex oligonucleotides directed against all transcripts of the mERG1 gene and RNAi-negative control duplex oligonucleotide (ncRNA) were provided by Invitrogen. The siRNA sequences were as follows: siRNA-1, 5′-AGG CUG ACA UCU GCC UAC ACC UGA A-3′; siRNA-2, 5′-UGU CAU UCC GCA GGC GUA CAG ACA A-3′. HL-1 cell culture of nearly confluent (passages 42–45) was transfected with siRNA against mERG1 or nonspecific RNA (ncRNA, 50 pmol), together with a reporter plasmid DNA (pEGFP vector, 0.5 µg) using Lipofectamine 2000 reagent (Invitrogen) according to the manufacture's instructions. Only GFP-positive cells 2 days after transfection were employed for electrophysiological experiments.

Patch-Clamp Recordings

Current recordings from HL-1 cells (passages 38–52) were performed using the whole-cell configuration of the patch-clamp technique (Hamill et al. 1981) with an EPC-8 patch-clamp amplifier (Heka, Lambrecht, Germany). Cells were dissociated from culture dishes by 0.05% trypsin/EDTA, suspended in Claycomb medium and stored at 4°C for a few hours before use. A small aliquot of cell suspension was transferred into a small (0.5 ml) recording chamber placed on the stage of an inverted microscope (TMD-300; Nikon, Tokyo, Japan). After settling to the glass bottom of the chamber (5–10 min), the cells were continuously superfused with normal Tyrode solution (containing appropriate drugs) kept at 25 ± 1°C or 35 ± 1°C, as indicated. Patch-clamp pipettes were prepared from glass capillary tube (Narishige, Tokyo, Japan) on a horizontal pipette puller (P-97; Sutter Instrument, Novato, CA), and the tips were then fire-polished by a microforge (MF-83, Narishige). Pipette resistance was 2–4 MΩ when filled with internal solution. Currents and voltages were digitized and voltage commands were generated through an ITC-16 AD/DA interface (InstruTECH, Long Island, NY) controlled by Pulse/Pulsefit software (version 8.54, Heka).

Data Analysis

Membrane capacitance (C_m) was calculated by fitting a single exponential function to the decay phase of the transient capacitive current in response to ±5-mV voltage steps (20 ms) from a holding potential of −50 mV. The current amplitude was divided by C_m to obtain the current density (pA pF^{-1}). Linear regression analysis was used for correlations. The voltage dependence of current activation and inactivation was determined by fitting the normalized

tail current (I_{tail}) vs. test potential (V) to a Boltzmann function expressed by $I_{tail} = 1/(1 + \exp[(V_{1/2} - V)/k])$ and $I_{tail} = 1/(1 + \exp[(V - V_{1/2})/k])$, respectively, where $V_{1/2}$ is the voltage at which the current is half-activated and k is the slope factor. The time constant for activation (τ_{act}) was determined from a single-exponential fit to the envelop of tail currents obtained after depolarizing pulses for varying durations, and time constants for deactivation (τ_{fast} and τ_{slow}) were obtained by fitting a two-exponential function to the time course of deactivating tail currents. Dose responses for drug block of currents were analyzed by fitting the relative amplitudes of tail currents (y/y_{max}) vs. the drug concentration ([D]) to a Hill function: $y/y_{max} = 1/\{1 + (IC_{50}/[D])^n\}$, where IC_{50} is the half-inhibitory concentration and n is the Hill coefficient. Data were expressed as mean ± SEM. Statistical analysis was performed by means of ANOVA and a post hoc Tukey test.

Solutions and Drugs

Normal Tyrode solution contained (mM) 140 NaCl, 0.33 NaH_2PO_4, 5.4 KCl, 1.8 $CaCl_2$, 0.5 $MgCl_2$, 5.5 glucose and 5 HEPES, pH adjusted to 7.4 with NaOH. The external solution for current recording was made by adding 0.4 μM nisoldipine (as 1 mM stock solution in ethanol) to normal Tyrode solution to eliminate $I_{Ca,L}$. In some experiments, the concentration of KCl was modified to 2 or 10 mM. The internal pipette solution contained (mM) 70 potassium aspartate, 50 KCl, 10 KH_2PO_4, 1 $MgCl_2$, 3 Na_2–ATP, 0.1 Li_2–GTP, 5 EGTA and 5 HEPES, pH adjusted to 7.2 with KOH. Liquid junction potential between the test solution and the pipette solution was measured at around −10 mV and corrected. In order to rule out possible contamination of $I_{Ca,L}$ in our data, all experiments were conducted in the presence of 0.4 μM nisoldipine (a generous gift from Bayer AG, Wuppertal-Elberfeld, Germany), which is specific blocker of $I_{Ca,L}$. E-4031 (Wako), dissolved in distilled water (1 mM) and dofetilide (a generous gift from Pfizer, Sandwich, UK), dissolved in acidified water (pH 4.0, 1 mM), were diluted down to the final concentration in the test solution.

Results

E-4031-Sensitive Current in HL-1 Cells

I_{Kr} was originally identified as a methanesulfonanilide-sensitive component of I_K in guinea pig cardiomyocytes (Sanguinetti and Jurkiewicz 1990). We recorded whole-cell membrane currents from single HL-1 cells before and after application of E-4031 and then analyzed a drug-sensitive current (Fig. 1). Possible participation of other voltage-dependent currents in our data was minimized; i.e., 0.4 μM nisoldipine was included in the bath solution to block $I_{Ca,L}$ (Xia et al. 2004) and membrane potential was held at −50 mV to inactivate $I_{Ca,T}$ (Xia et al. 2004) and avoid I_f activation (Sartiani et al. 2002). Figure 1a shows representative membrane currents in response to 1-s depolarizing (upper panel) and hyperpolarizing (lower panel) pulses to various test potentials, ranging between −80 and +40 mV in 10-mV steps from a holding potential of −50 mV. As shown in the upper panel of Fig. 1a, depolarizing steps activated time-dependent outward currents with amplitudes that increased with depolarization up to 0 mV and then progressively decreased as the potential became more positive (filled circles, Fig. 1d). After return of the membrane to the holding potential, slowly deactivating tail currents were elicited. In contrast, as shown in the lower panel, hyperpolarizing steps induced small-amplitude inward currents with a slight time dependence, which was possibly due to activation of I_f channels, and following depolarizing steps to the holding potential elicited transient inward currents, which may be attributed to activation of $I_{Ca,T}$. When E-4031 (5 μM) was applied to the bath solution, the time-dependent outward current during depolarizing steps as well as the tail current were almost completely abolished, whereas the inward current during the hyperpolarizing pulse was not significantly influenced (Fig. 1b). The currents after exposure to the drug were nearly time-independent and exhibited small conductance with slight outward rectification (open circles in Fig. 1d). E-4031-sensitive currents obtained by digital subtraction of current traces in the presence of drug from those before application of the drug are illustrated in Fig. 1c. The drug-free and the E-4031-sensitive currents showed very similar current–voltage relationships, and both currents have the characteristics of inward rectification at more positive potential than 0 mV, indicating that I_{Kr} is the dominant outward current in HL-1 cells.

The voltage dependence for I_{Kr} activation was determined by measuring the tail amplitude of E-4031-sensitive current. Figure 2a shows the initial part of tail currents elicited upon return of the membrane potential to −50 mV from the 1-s depolarizing steps to test potentials ranging from −40 to +40 mV. The tail current obviously activated at −30 mV and increased in amplitude for the steps up to +10 mV. In Fig. 2b, the amplitude of the tail currents was normalized to the maximum tail current amplitude and plotted as a function of the membrane potential. The $V_{1/2}$ and k, which were determined by curve fitting the data points to a Boltzmann equation, were −20.4 and 8.0 mV, respectively.

In Fig. 3, kinetic properties were determined by measuring time constants for apparent activation and deactivation of I_{Kr}. An envelope-of-tails test was used to assess

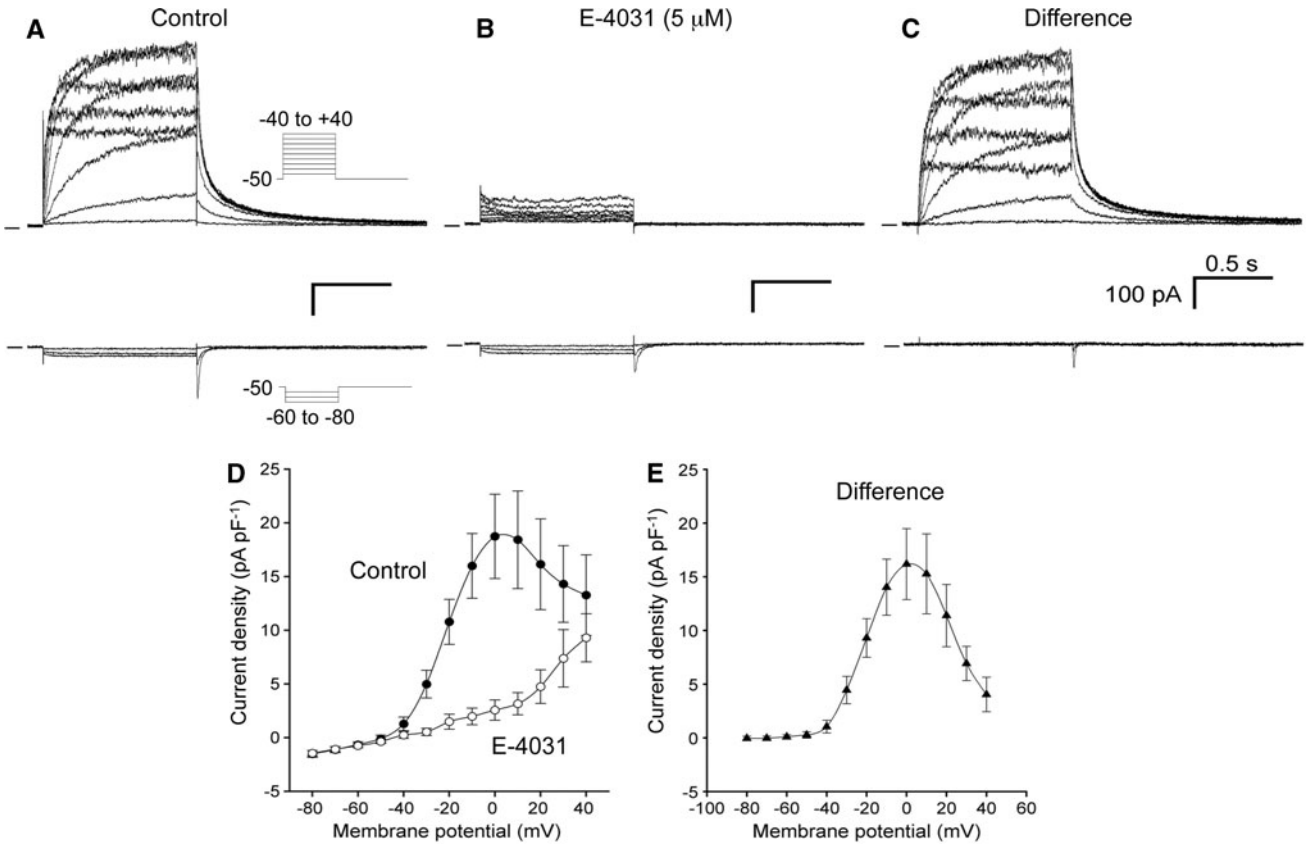

Fig. 1 E-4031-sensitive current recorded from isolated HL-1 cells. **a**, **b** Superimposed whole-cell membrane currents recorded from single HL-1 cell (passage 38) before (**a**) and after (**b**) exposure to 5 μM E-4031. The cell was held at −50 mV and given 1-s depolarizing (between −40 and +40 mV, *upper panel*) and hyperpolarizing (between −80 and −60 mV, *lower panel*) test pulses. The experiment was conducted at 35°C. **c** E-4031-sensitive current obtained from digital subtraction of two traces in **a** and **b**. **d** Average current–voltage relationships recorded before (*filled circles*) and after (*open circles*) exposure to E-4031. Current amplitudes measured just before the end of the 1-s pulses were plotted against the indicated membrane potentials. Values represent mean ± SEM of 10 HL-1 cells (passages 38–41). **e** Current–voltage relationship for E-4031-sensitive currents

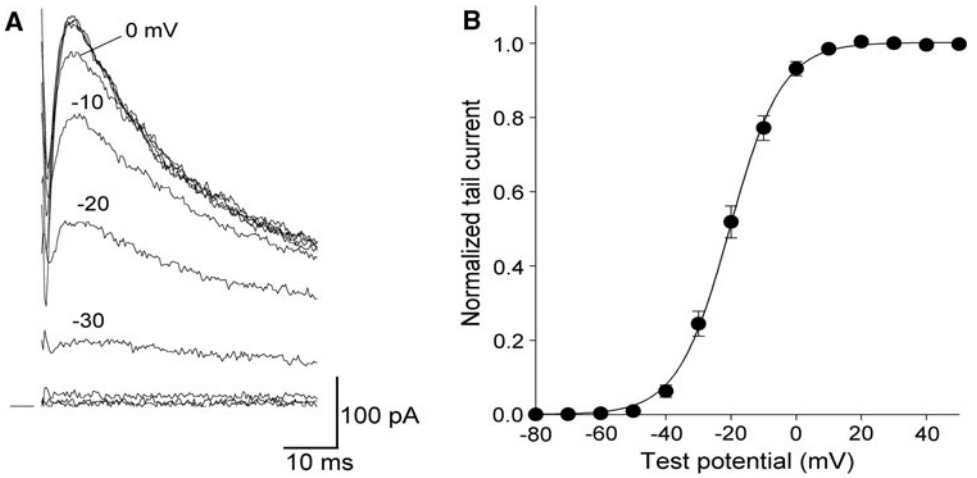

Fig. 2 Voltage-dependent activation of E-4031-sensitive current in HL-1 cells. **a** Representative tails of E-4031-sensitive current recorded from an HL-1 cell (passage 38). Tail currents were elicited on repolarization to −50 mV, following 1-s depolarization to +20 mV. **b** Voltage dependence of E-4031-sensitive current. Tail current amplitudes were normalized to the maximal value at +20 mV, and averaged data were plotted against the indicated test potentials. Values represent mean ± SEM of 10 HL-1 cells (passages 38–41). *Smooth curve* represents fitting of the data to the Boltzmann equation

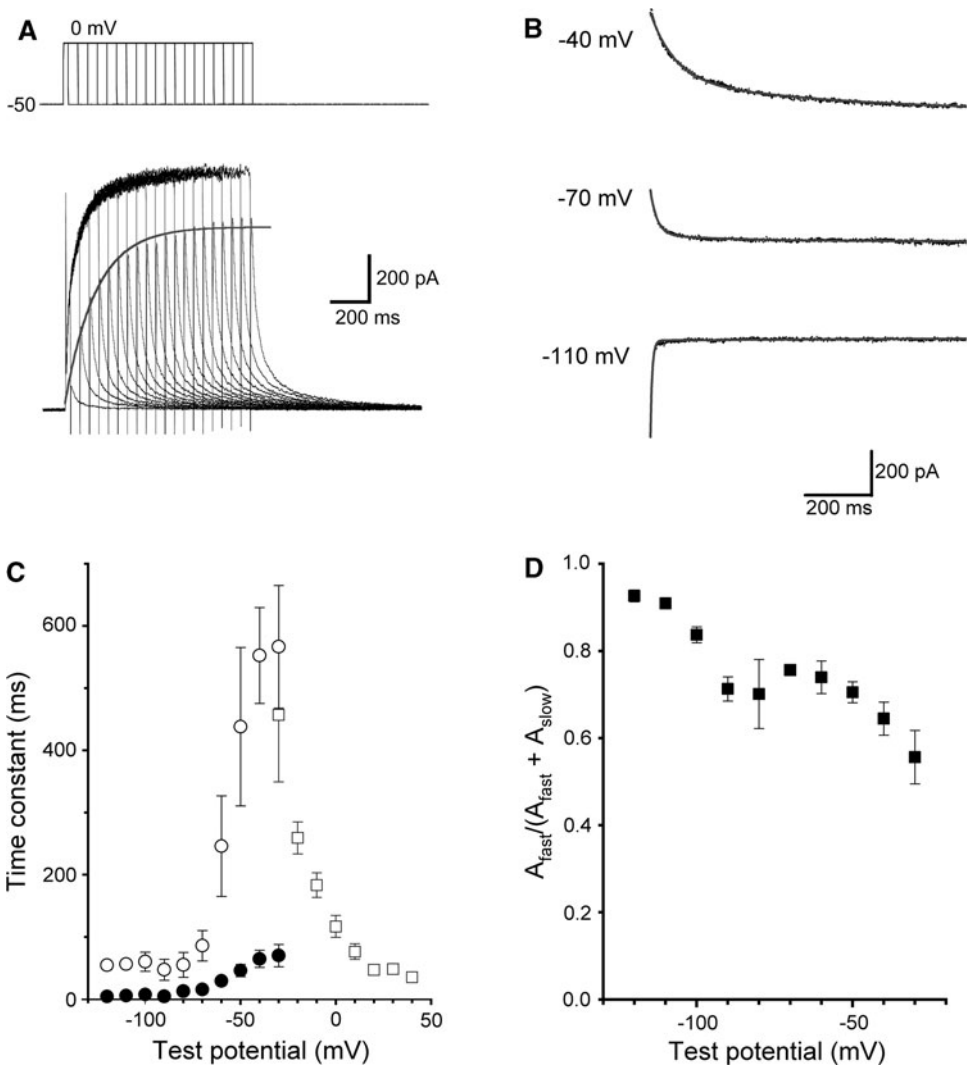

Fig. 3 Activation and deactivation kinetics. **a** Activation time courses assessed with an envelope-of-tails protocol. Original current traces recorded from an HL-1 cell (passage 44) in response to the depolarizing steps to 0 mV of varying duration (25–975 ms in 50-ms increments) from a holding potential of −50 mV. *Solid curve* is a single-exponential fit to the peak tail current elicited upon repolarization to the holding potential. **b** Deactivation time courses of E-4031-sensitive current recorded from an HL-1 cell (passage 39). Decaying phase of tail currents (*dots*) elicited at −40, −70 and −110 mV after depolarizing prepulse to +20 mV of 1-s duration were fit to a sum of two exponential equations (*solid line*). **c** Average voltage dependence of time constants for the apparent activation (*open squares*) and the fast (*open circles*) and slow (*filled circles*) components of deactivation of the E-4031-sensitive current. **d** Voltage dependence of the relative amplitude of the fast component in decaying tail current. Values represent mean ± SEM of four to 10 cells (passages 38–47)

the time course of activation. Figure 3a shows a representative example of current traces in response to depolarizing test pulses to 0 mV of varying duration (25–975 ms in 50-ms increments). The tail current amplitude on return to the holding potential reflects the extent of I_{Kr} activation produced during depolarization to 0 mV, which was well fitted by a single-exponential function, where the τ value was 162.8 ms. The kinetics was steeply voltage-dependent and the activation time constants decreased with incremental changes in the test potentials (τ_{act}, open squares in Fig. 3c). Time constants of deactivation were calculated by fitting the decay of tail currents at various test potentials between −120 and −20 mV following 1-s depolarizing pulses to +20 mV to a double-exponential function, as shown in Fig. 3b. In contrast to activation, the deactivation time course was accelerated at more negative potentials. As summarized in Fig. 3c, both the fast (τ_{fast}, filled circles) and slow (τ_{slow}, open circles) time constants of deactivation were increased as the test potential became more positive. The slow time constants of deactivation at −30 mV were comparable to the time constant of activation at the same potential, and they were plotted as a bell-shaped function of the membrane potential. Figure 3d shows a plot of the relative amplitude of the fast component, $A_{fast}/(A_{fast} + A_{slow})$, of decaying tail current against the membrane potential. The value decreased from approximately 0.9 to 0.5 over the membrane potential from −120 to −20 mV.

I_{Kr} Density in HL-1 Cells

There was a large cell-to-cell variation in HL-1 cell size even in the same culture; C_m measured in patch-clamp experiments ranged between 5.4 and 84.0 pF (mean ± SEM, 29.9 ± 2.3 pF). We tested whether ununiformity of cell size reflects their functional heterogeneity of I_{Kr} channel. The relationship between I_{Kr} density and C_m was investigated in 69 cells (Fig. 4a). The I_{Kr} density ranged between

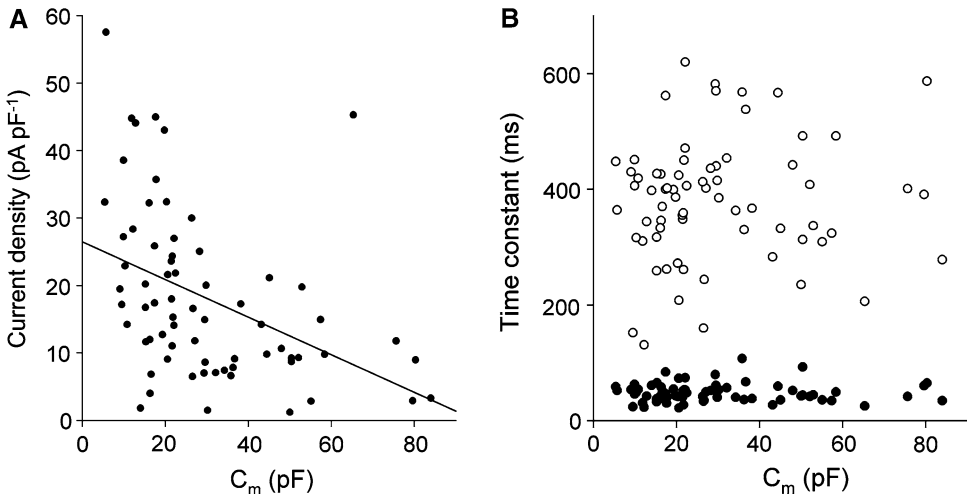

Fig. 4 Relationships between HL-1 cell size and E-4031-sensitive current. Scatter plots of the current density (**a**) and the deactivation time constants (**b**) of the slow (*open circles*) and fast (*filled circles*) components, measured in E-4031-sensitive tail current elicited by a voltage step to −50 mV after 1-s depolarization to +20 mV, against the membrane capacitance of individual cells. Data were obtained from HL-1 cells (passages 38–52)

1.2 and 57.5 pA pF^{-1} (18.1 ± 1.5 pA pF^{-1}, $n = 69$), which was roughly and negatively correlated with cell size ($r = -0.42$, $P < 0.0003$). On the other hand, no obvious correlation between deactivation kinetics of I_{Kr} and cell size was observed (Fig. 4b).

Voltage Dependence of I_{Kr} Inactivation in HL-1 Cells

The shape of the I_{Kr} tail current (initial "hook" or increase in amplitude, followed by slower decay) reflects the presence of a biphasic process during repolarization. The initial increasing phase of the tail current preceding a decay in amplitude has been shown to reflect a recovery from inactivation that occurs much faster than deactivation (Sanguinetti and Jurkiewicz 1990; Shibasaki 1987). In Fig. 5, the rate of recovery from inactivation was estimated. The currents were elicited by voltage pulses to various test potentials between −120 and −10 mV after the 1-s preconditioning pulses to +20 mV. Experiments were conducted at 25°C to allow discrimination of the onset of tail currents from capacitive transients. In Fig. 5a, a set of current traces during test steps is shown. Increment phases of the tail current were well fitted by a single-exponential function with smaller time constants at more negative potentials. For example, the averaged τ value at −120 mV was 0.92 ± 0.04 ms, while it increased to 10.50 ± 0.74 ms at −10 mV (Fig. 5b).

The voltage dependence of current inactivation was examined using a three-pulse protocol (inset in Fig. 6a) (Smith et al. 1996), in which the cell was depolarized to +20 mV for 1 s to activate and inactivate I_{Kr} channels,

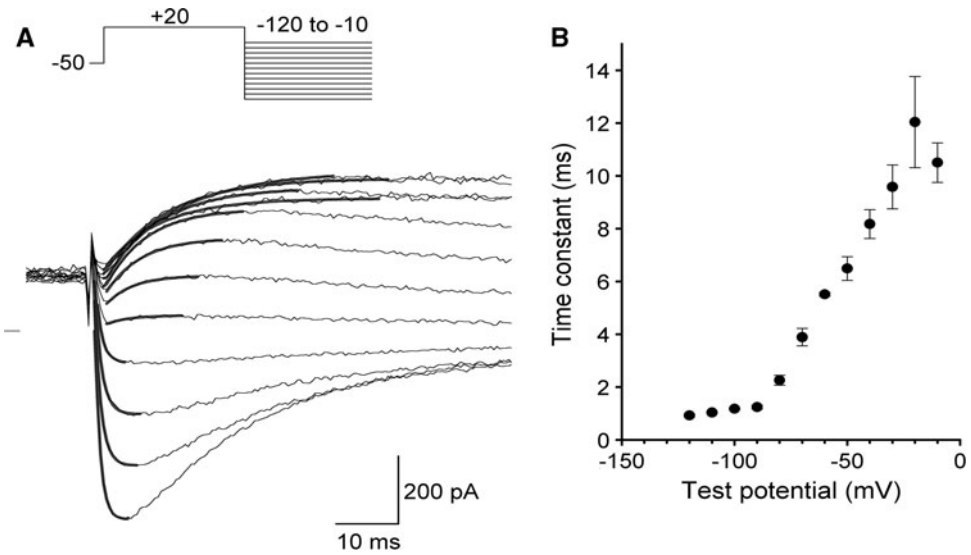

Fig. 5 Kinetic properties of recovery from inactivation. **a** The "hook" tail currents (*thin line*) elicited by voltage steps to various potentials between −120 and −10 mV in 10-mV intervals following the 1-s depolarizing steps to +20 mV (*inset*). Current recording was conducted at 25°C. *Smooth curves* (*thick line*), superimposed to initial increasing phase in amplitude, are obtained by a single-exponential fit. **b** Voltage dependence of the rate of recovery from inactivation. Time constants, measured in (**a**), were plotted against each test potential. Values represent mean ± SEM of four cells (passages 41, 42)

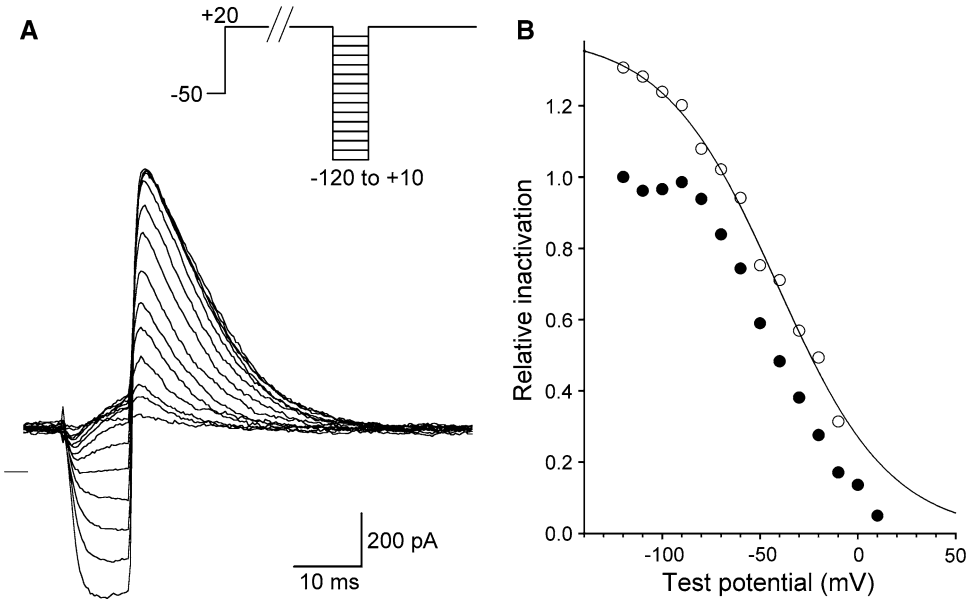

Fig. 6 Voltage dependence of steady-state inactivation. **a** E-4031-sensitive current recorded from an HL-1 cell (passage 41) in response to three-pulse protocol (*inset*). At first, a depolarizing pulse of more than 1 s duration to +20 mV (P1) was applied, where current was activated and inactivated rapidly. Then, a hyperpolarizing test pulse of 10 ms to a varied potential (P2) was used to allow recovery from inactivation, followed by a step to +20 mV (P3). *Dashed line* represents zero current level. Current recording was conducted at 25°C. **b** Current amplitude in response to the P3 pulse (*filled circles*) was normalized to the maximal amplitude at −120 mV and plotted against the test potentials. At negative voltages (≤−60 mV), significant deactivation occurred during 10 ms of the P2 repolarizing step. In addition, at less negative potential (>−70 mV), increasing phase current did not reach the steady-state level during the P2 step. Therefore, the fractional deactivation and incomplete recovery from inactivation during 10 ms were calculated using kinetic parameters (obtained from current traces in Fig. 5), and the data points were corrected to the steady-state inactivation level (*open circles*). Corrected values were well fitted by the Boltzmann equation (*smooth curve*)

then briefly (10 ms) repolarized to various test potentials between −120 and +10 mV to allow for recovery from inactivation without significant deactivation of the channels. After the brief steps, a depolarizing step to +20 mV was applied to evaluate the relative number of opening channels. Figure 6a shows a part of the current traces in response to the pulse protocol (as indicated in the inset). During the brief repolarization, the currents relaxed rapidly to the appropriate level to the corresponding test potentials. Then, depolarizing pulses to +20 mV elicited a large amplitude of outward currents that decayed to the steady-state level within 40 ms due to rapid inactivation. The peak amplitude of the outward currents was measured and plotted against test potentials as filled circles in Fig. 6b. Smith et al. (1996) described that the current amplitude at negative voltages (≤−60 mV) should be corrected because fast deactivation occurred during the brief repolarization. Furthermore, the recovery from inactivation also might not reach the steady-state level at depolarized potential (>−70 mV). Thus, the fractional deactivation and recovery from inactivation during 10-ms repolarizing steps were corrected with respect to the steady-state inactivation level (open circle in Fig. 6b). The half-maximal inactivation voltage calculated by fitting the corrected data to a Boltzmann function was −41.2 mV and the slope factor was 28.9 mV.

K^+ Permeability of I_{Kr} in HL-1 Cells

In Fig. 7, the effects of $[K^+]_o$ on the reversal potential (E_{rev}) of the tail current were investigated. Cells were bathed in Tyrode solution containing 2, 5.4 (normal) and 10 mM KCl; and tail currents were recorded at various test potentials between −120 and 0 mV in 10-mV steps following the 1-s preconditioning pulses to +20 mV (Fig. 7a). The tail current amplitudes were measured and plotted against test potentials in Fig. 7b. At all $[K^+]_o$ conditions, the current–voltage relationships were nearly linear at the potential range between −140 and −80 mV and prominent inward rectification was observed at more positive potential than −70 mV. The conductance at potentials between −140 and −80 mV, measured by fitting lines with a liner regression, was increased with incremental change in $[K^+]_o$ (10.6, 14.1 and 19.7 pS at 2, 5.4 and 10 mM $[K^+]_o$, respectively). E_{rev}, where the polarity of the tail current is reversed, was obtained from a linear regression of the data points between −140 and −70 mV. E_{rev} values at 2, 5.4 and 10 mM $[K^+]_o$ were −115, −91 and −76 mV, respectively, very near the calculated

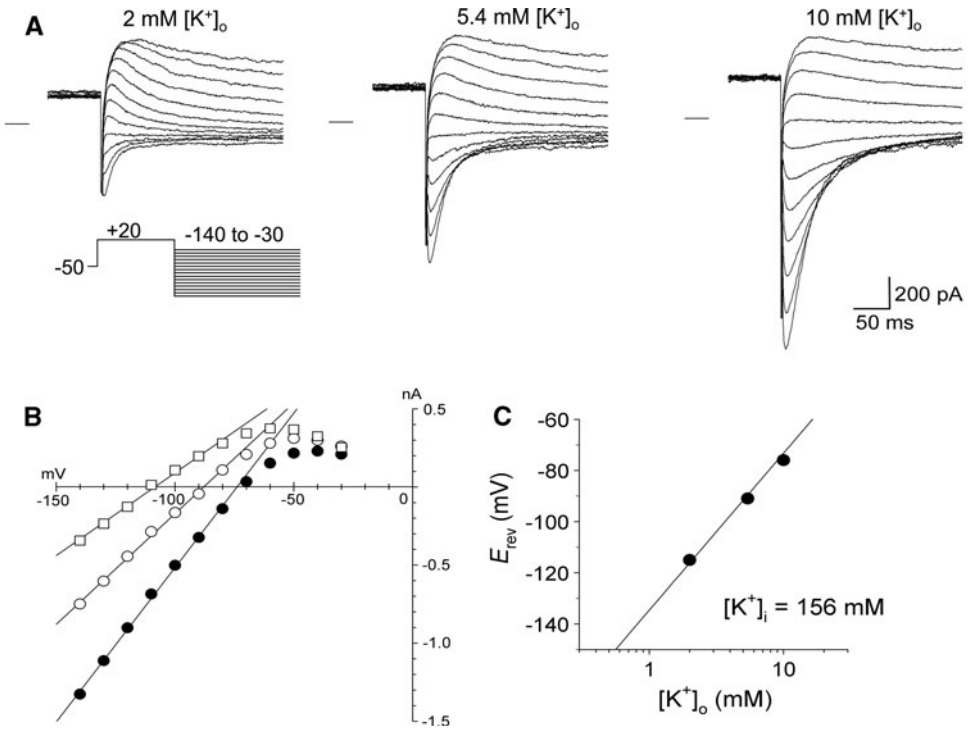

Fig. 7 Effects of extracellular K^+ concentrations on E-4031-sensitive currents. **a** Tail currents recorded at 2 (*left*), 5.4 (*middle*) and 10 mM $[K^+]_o$ conditions (*right*) at 25°C. The cell (passage 39) was initially depolarized to +20 mV from a holding potential of −50 mV, followed by test steps to various potentials between −120 and −30 mV (voltage protocol, *inset*). **b** Tail current amplitude at 2 (*open squares*), 5.4 (*open circles*) and 10 mM $[K^+]_o$ conditions (*filled circles*) shown as a function of test potentials. *Solid lines* on the plot were obtained by a linear regression of data points between −140 and −70 mV: $I_{tail} = g_{max} \cdot (E - E_{rev})$, where g_{max} and E_{rev} were, respectively, 10.6 pS and −115 mV at 2 mM $[K^+]_o$, 14.1 pS and −91 mV at 5.4 mM $[K^+]_o$ and 19.7 pS and −76 mV at 10 mM $[K^+]_o$. **c** Relationships between $[K^+]_o$ and E_{rev}. E_{rev} values in (**b**), plotted against each $[K^+]_o$ concentration, were in good agreement with a predicted E_K (*solid line*) calculated using a Nernst equation, $E_K = RT/F \cdot \ln([K^+]_o/[K^+]_i)$, where $[K^+]_i$ was assumed to be 158 mM

equilibrium potential of K^+ of −116, −89 and −73 mV, respectively (Fig. 7c).

Blocking Effects of E-4031 and Dofetilide on I_{Kr} in HL-1 Cells

In Fig. 8, the blocking effects of methanesulfonanilide drugs E-4031 and dofetilide on I_{Kr} in HL-1 cells were determined. The 1-s depolarizing pulses to +20 mV were repetitively given to the cells every 8 s to activate I_{Kr}, and the blocking effects of the drugs were determined by reduction of tail current elicited at −50 mV. Figure 8a shows the time course of changes in tail current amplitude during application of E-4031 at various concentrations as indicated. In the absence of drugs, the magnitude of the tail current was stable. Exposure to 10 nM E-4031 gradually reduced the tail currents by about 20% at the steady-state level, and the blocking effects increased as the drug concentration became higher. The IC_{50} values for block of tail currents by dofetilide and E-4031 were estimated to be 15.1 and 21.2 nM, respectively; and both drugs inhibited tail current completely at 1 μM (Fig. 8b, c).

Mouse ERG1 Expression Underlies I_{Kr} in HL-1 Cells

In Fig. 9, mERG1 expression in HL-1 cells was investigated with RT-PCR and Western blot assay. It has been reported that there are at least three isoforms of ERG1 at the mRNA level in human and mouse, i.e., the full-length ERG1a and two alternative splicing variants, ERG1a′ and ERG1b, with shorter N termini (Lees-Miller et al. 1997; London et al. 1997). In the present study, therefore, primer pairs directed to each ERG1 isoform were used for PCR amplification. Figure 9a shows an agarose gel of amplified PCR products, where specific bands of the expected size are detected for mERG1a (747 bp), mERG1a′ (755 bp) and mERG1b (1,109 bp) only in the presence of transcriptase. A similar gene expression profile was also detected in adult mouse atrial tissue (Fig. 9b). In order to examine protein expression, we employed an anti-ERG1 antibody that recognizes a common C-terminal epitope in all three mERG1 isoforms. As shown in Fig. 9c, the C-terminal ERG1 antibody identified several bands on a Western blot of HL-1 cells. The two higher bands with molecular mass of 120 and 160 kDa are consistent with maturely

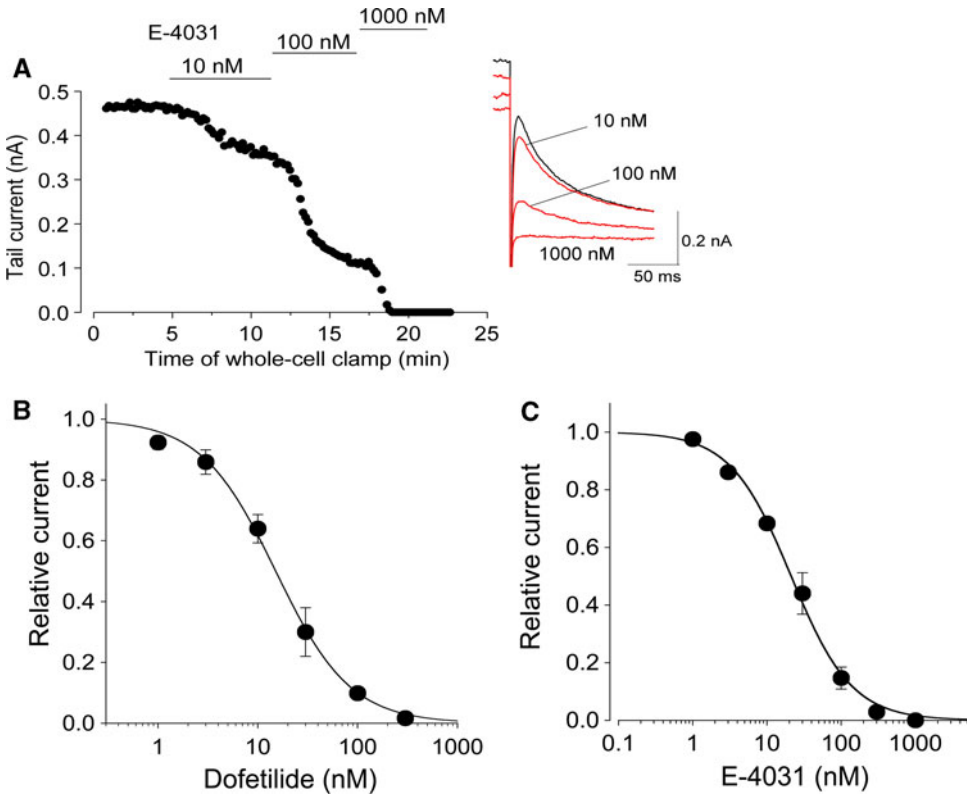

Fig. 8 Inhibitory effects of E-4031 and dofetilide on I_{Kr} in HL-1 cells. **a** Time course of changes in tail current amplitude during exposure to E-4031. Tail currents, as shown in *inset*, were elicited by a voltage step to −50 mV after 1-s depolarization to +20 mV. E-4031 was applied at various concentrations as indicated. **b**, **c** Dose-response relationships of blocking effects of E-4031 (**b**) and dofetilide (**c**). Tail current amplitude was normalized to the maximal amplitude in the absence of drug and plotted against each drug concentration. Data points represent mean ± SEM of five cells (passages 41–52). *Smooth curve* was obtained by fitting the data with a Hill equation, where IC_{50} and Hill coefficient were, respectively, 15.1 nM and 1.2 in (**b**) and 21.2 nM and 1.0 in (**c**)

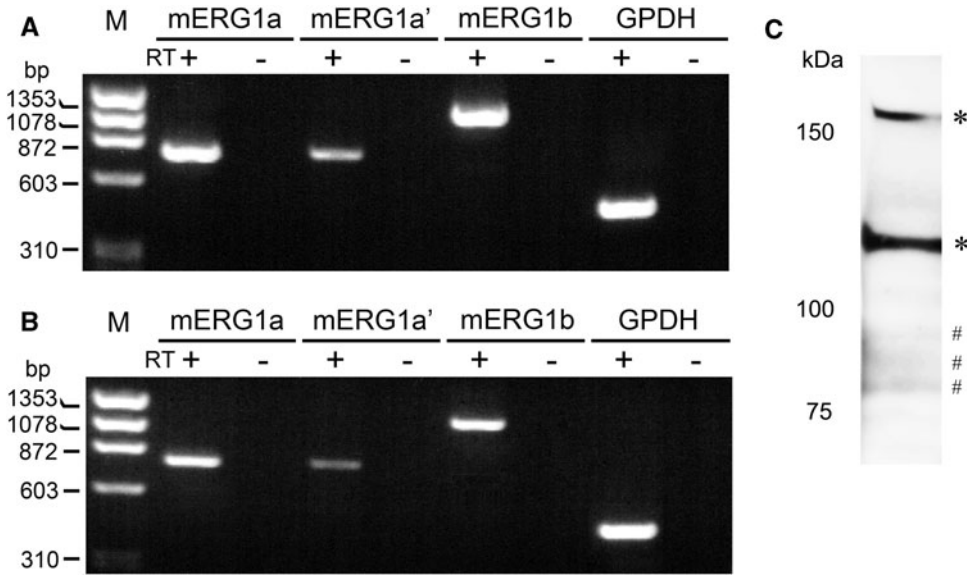

Fig. 9 Expression of mouse ERG1 isoforms in HL-1 cells and mouse atrium. PCR products amplified from cDNA derived from HL-1 cells culture (passage 40) (**a**) and atrial tissues dissected from adult mice (**b**), using primer pairs directed to mERG1a, mERG1a′ or mERG1b. *M* indicates a molecular maker of ϕX174/*Hae*III digest. **c** Western blot of total protein extracts from HL-1 cells (passages 45–47). Blotting with an antibody specific for ERG1 shows two mERG1a glycoform bands (*) at 120 and 160 kDa as well as three mERG1b glycoform bands (#) at 80, 87 and 93 kDa

glycosylated and unglycosylated ERG1a, respectively, in rat and canine ventricular myocytes (Jones et al. 2004), although contamination of signal attributed to ERG1a′ may be possible because of a small difference (∼6 kDa) in protein size. On the other hand, we did observe three faint bands with lower molecular mass of 80, 87 and 93 kDa, which are consistent with bands attributed to different glycosylated forms of ERG1b in human and canine ventricular myocytes (Jones et al. 2004) and K562 human leukemic cells (Cavarra et al. 2007).

Recently, gene silencing by RNAi has become a broadly used technology for exploring gene function (Hannon 2002). In the present study, the functional relevance of mERG1 gene expression in HL-1 cells was determined using the RNAi technique. Two siRNA duplex oligonucleotides against all isoforms of mERG1 and ncRNA were

individually transfected into HL-1 cells together with a plasmid vector encoding GFP. Transfection efficacy estimated with green fluorescence was very low (≤5%), which never allowed us to detect an obvious decrease in mERG1 transcripts or proteins at the culture level (data not shown). However, the effects of siRNA were evident in whole-cell membrane current recorded from single GFP-positive cells. Compared to recordings in cells transfected with GFP alone (Fig. 10a), a much smaller time-dependent outward current was observed in cells transfected with siRNA, apparently due to a marked decrease in I_{Kr} amplitude (Fig. 10c, d). The effect of siRNA was attributable to specific knockdown of mERG1 expression because cells transfected with scRNA displayed currents with comparable amplitude to those recorded from cells transfected with GFP alone (Fig. 10b). I_{Kr} density determined by tail current elicited at −50 mV after the 1-s voltage steps to +30 mV was 1.95 ± 0.31 and 1.2 ± 0.34 pA pF^{-1} in cells transfected with siRNA-1 and siRNA-2, respectively. Both values were significantly smaller than those obtained from cells transfected with GFP alone (19.15 ± 2.34 pA pF^{-1}, $P < 0.01$) or with ncRNA (19.00 ± 2.69 pA pF^{-1}, $P < 0.01$) (Fig. 10e).

Discussion

In this article we describe the basic biophysical properties and molecular identity of I_{Kr} channels in HL-1 cells, the unique murine cardiac cell line established by Claycomb et al. (1998). Our current recordings demonstrated that most of the outward conductance in these cells was dominated by E-4031-sensitive current, which exhibited comparable characteristics to I_{Kr} in native mammalian cardiac cells, i.e., voltage- and time-dependent activation, prominent inward rectification, high K^+ permeability and nanomolar sensitivity to dofetilide or E-4031. In addition, we found that HL-1 cells possessed multiple transcripts and

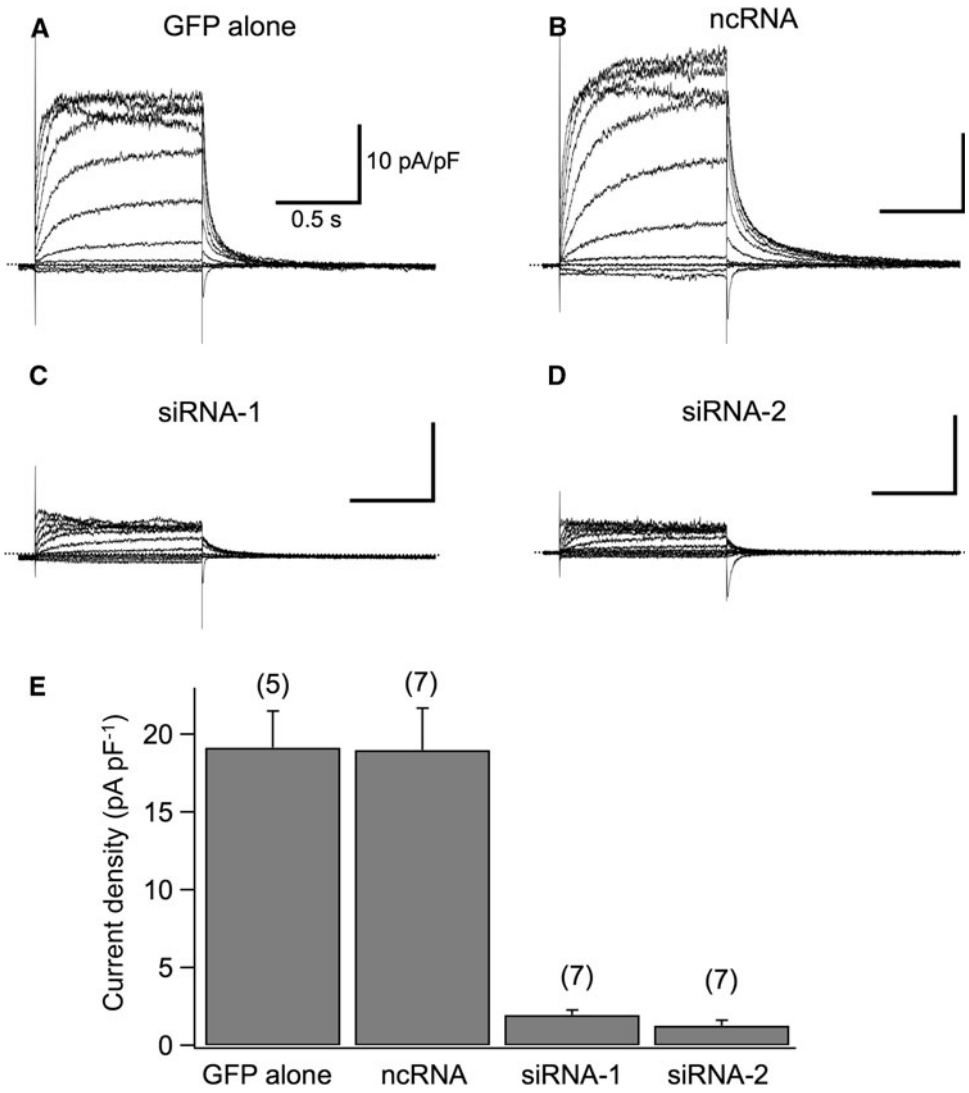

Fig. 10 Knockdown of mouse ERG1 with siRNA in HL-1 cells. Typical current traces recorded from HL-1 cells (passages 40, 41) transfected with GFP alone (**a**), GFP and nonspecific ncRNA (**b**), GFP and siRNA-1 (**c**) and GFP and siRNA-2 (**d**). Cell was held at −50 mV and given 1-s voltage steps to various potentials between −80 mV and +40 mV. **e** Bar graph displaying I_{Kr} density in each group (GFP alone, $n = 5$; GFP plus ncRNA, $n = 7$; GFP plus siRNA-1, $n = 7$; GFP plus siRNA-2, $n = 7$). Tail current was elicited upon repolarization to −50 mV following the 1-s depolarizing steps to +30 mV

proteins for the mouse ERG1 gene, known as molecular candidates underlying I_{Kr}. These findings indicate that HL-1 cells are a preferable source of native I_{Kr} channels.

Biophysical and Pharmacological Properties of I_{Kr} in HL-1 Cells

The biophysical profile of I_{Kr} channels is responsible for their specific role in cardiac action potential. The inward rectification mediated by a rapid voltage-dependent inactivation of channels suppresses current during the depolarizing phase of cardiac action potential, while a rapid recovery from inactivation followed by slow deactivation evokes a resurgent current during phase III repolarization. These unique gating properties have been extensively investigated in HERG channels. However, despite its physiological importance, relatively little information on cardiac I_{Kr} channels is available due to technical difficulties; i.e., significant current magnitude and minimal contamination of other time-dependent K^+ currents are required for reliable measurements. Current recordings in HL-1 cells potentially satisfied these requirements, which allowed us to evaluate the electrophysiological properties of I_{Kr} channels comprehensively. One possible limitation in our I_{Kr} recordings was that a holding potential of −50 mV was used to avoid contamination of $I_{Ca,T}$ (Xia et al. 2004) and I_f (Sartiani et al. 2002), which might affect I_{Kr} kinetic parameters and drug sensitivity because a significant fraction of channels were restrained in the inactivated state at −50 mV (see Fig. 6). Nevertheless, our recordings are similar to ones applying common protocols for the recording of native I_{Kr} in cardiomyocytes; thus, it is possible to draw a comparison between our results and those of earlier studies.

Voltage dependence of I_{Kr} activation in HL-1 cells was determined by two parameters, $V_{1/2}$ of −20.4 mV and k of 8.0 mV, which are practically consistent with the values previously reported for cardiac I_{Kr} in various mammals (Clark et al. 2004; Matsuura et al. 2002; Ono and Ito 1995; Sanguinetti and Jurkiewicz 1990). The deactivation kinetics of I_{Kr} varies between species. It is fast in guinea pig (Sanguinetti and Jurkiewicz 1990), while it is extremely slow in dog and cat (Barajas-Martínez et al. 2000; Liu and Antzelevitch 1995). In the present study, deactivation time constants were 46 ms for τ_{fast} and 438 ms for τ_{slow} at −50 mV when fitted to a double-exponential function, which are very similar to recent observation in mouse SA node cells (τ_{fast} and τ_{slow} were 40–70 ms and 400–600 ms at −50 mV, respectively) (Clark et al. 2004). Recovery from inactivation was very rapid even at 25°C, and time constants obtained in HL-1 cells were comparable to previous data for I_{Kr} in ferret atrial cells (Liu et al. 1996) but considerably smaller than the observation for HERG currents (Sanguinetti et al. 1995). We also determined the voltage dependence of steady-state inactivation of I_{Kr} channels using a three-pulse protocol that has been employed for HERG currents (Smith et al. 1996). The $V_{0.5}$ of −41.2 mV obtained in our analysis was very far from the value with HERG current (−90 mV) (Smith et al. 1996) but relatively similar to the value estimated by other methods in guinea pig or ferret (Liu et al. 1996; Sanguinetti and Jurkiewicz 1990), suggesting fundamental differences between cardiac I_{Kr} and HERG current in inactivation properties. Taken together, HL-1 cells appear to retain species-specific features of native I_{Kr}.

The sensitivity of I_{Kr} in HL-1 cells to E-4031 (IC_{50} 21.1 nM) was similar to that reported for native I_{Kr} in ferret and guinea pig cardiomyocytes (IC_{50} ∼10 nM) (Liu et al. 1996; Weerapura et al. 2002). Dofetilide sensitivity observed in the present study (IC_{50} 15.1 nM) was also comparable with the values reported for native I_{Kr} in rabbit and guinea pig cardiomyocytes (IC_{50} 4–9 nM) (Carmeliet 1992; Weerapura et al. 2002). The sensitivity of the HERG channel to these compounds varies among expression systems. The channel expressed in *Xenopus* oocytes displays much lower sensitivity (E-4031 IC_{50} ∼1 μM) (Sanguinetti et al. 1995), possibly due to yolk sac absorption of drugs in oocytes (Weerapura et al. 2002). On the other hand, in mammalian cell lines such as HEK cells and CHO cells, the IC_{50} values for the inhibition of HERG channel by E-4031 and dofetilide were reported to be 7.7 and ∼10 nM, respectively (Zhou et al. 1998; Weerapura et al. 2002), which are indistinguishable from those previously reported for native I_{Kr} as well as our observation in HL-1 cells. Since inhibition of I_{Kr} is the predominant adverse effect of a diverse range of therapeutic agents (resulting in life-threatening proarrhythmic activity), assay of I_{Kr} in HL-1 cells may serve as a convenient preclinical tool to detect potential arrhythmogenic properties of any compound intended to be used as human medicine.

HL-1 Cells Possess Electrophysiological Properties Resembling Embryonic Phenotypes

Cardiac I_K is known to comprise at least two components, I_{Kr} and I_{Ks}, in various mammals. In HL-1 cells, however, I_{Kr} seems to be the sole I_K component. Indeed, a time-dependent outward current was almost totally abolished by application of E-4031 (Fig. 1). In mouse ventricular myocytes, the expression level of I_{Kr} and I_{Ks} is dependent on the developmental stage (Wang and Duff 1996; Wang et al. 1996); i.e., I_{Kr} is the predominant component of I_K in embryonic and fetal mice but is decreased during early postnatal development, whereas I_{Ks} is increased and both currents almost disappear in adult mouse. Along with these finding, the I_{Kr} expression pattern of HL-1 cells appears to

be similar to that of immature fetal mouse myocytes rather than well-differentiated adult mouse myocytes, although they derived from adult mouse hearts. Similarly, a fetal-type electrophysiological phenotype of HL-1 cells has been indicated by the expression of I_f and $I_{Ca,T}$ (Sartiani et al. 2002; Xia et al. 2004), which are known to be manifested in ventricular myocytes only at early embryonic stages (Niwa et al. 2004; Yasui et al. 2001).

HL-1 cells are known to beat when grown at proper density, again resembling embryonic cardiomyocytes. The spontaneous contractile activity, however, occurs in a restricted region of culture (Sartiani et al. 2002), suggesting heterogeneity of the functional expression level of ion channels in HL-1 cells. In fact, I_f was observed in only ~30% of HL-1 cells (Sartiani et al. 2002). Interestingly, the presence of both $I_{Ca,L}$ and $I_{Ca,T}$ had similar incidence (Xia et al. 2004). The limited expression of these membrane currents seems to be in agreement with the partial (local) occurrence of spontaneous beating in HL-1 cell culture because they play crucial roles in cardiac pacemaker activity. In the present study, I_{Kr} was recorded in almost all cells tested, even in quiescent HL-1 cells, while the current density of I_{Kr} was roughly and significantly correlated with cell size (Fig. 4). It has been suggested that a cell size-dependent difference in expression level of various ionic currents underlies the regional difference in electrical activity of rabbit SA node (Honjo et al. 1996; Lei et al. 2001). Although the relationship between spontaneous activity and the size of HL-1 cells is not known, it may be that the expression level of I_{Kr} channels is involved in the capability of spontaneous beating in HL-1 cell culture.

Molecular Basis of I_{Kr} in HL-1 Cells

The molecular basis of native I_{Kr} channel is still in debate. Although there is little doubt that the ERG1 gene underlies I_{Kr} channels in the heart, the reconstituted HERG channel displays much slower deactivation kinetics than native I_{Kr} channels (Sanguinetti et al. 1995). For this reason, auxiliary subunits such as KCNE1 and KCNE2 have been implicated as functional regulators of HERG channel (Abbott et al. 1999; McDonald et al. 1997). According to our preliminary experiments, we detected mRNA for KCNE1 from HL-1 cells, consistent with previous observations in AT-1 cells (Yang et al. 1994), but failed to find obvious expression of KCNE2 (data not shown). On the other hand, N-terminal splice variants of the ERG1 gene have been cloned in mouse and human and suggested to generate functional diversity of native I_{Kr} channels (Lees-Miller et al. 1997; London et al. 1997). The importance of these variants in the human heart was recently highlighted by the finding of a HERG1b-specific missense mutation associated with long QT syndrome (Sale et al. 2008). The N-terminal region of ERG1 contains the Per-Arnt-Sim (PAS) domain, which plays a crucial role in the slow deactivation process of the channel (Morais Cabral et al. 1998). The ERG1b isoform, which lacks the PAS domain in its truncated N terminus, exhibits faster deactivation than the full-length ERG1a (London et al. 1997), although its surface expression is not efficient unless coassembled with ERG1a (Phartiyal et al. 2007). In heterologous systems, coexpression of ERG1a and ERG1b leads to formation of a functional heterotetrameric channel with deactivation properties that more closely resemble native I_{Kr} than the channels produced by the expression of these isoforms individually (London et al. 1997). In fact, the deactivation time course of I_{Kr} in HL-1 cells was more similar to that reported for the mERG1a/1b channels rather than the mERG1a homomeric channel (e.g., τ_{fast} and τ_{slow} at −50 mV were 46 and 438 ms, respectively, in our experiments compared to 400–500 and ~2,000 ms, respectively, in mERG1a channel and 70–80 and 400–600 ms, respectively, in mERG1a/1b channel [London et al. 1997]). In the present study, we also confirmed the expression of both mERG1a and mERG1b in HL-1 cells, supporting the possible contribution of these isoforms in producing I_{Kr} in HL-1 cells. However, despite the abundance of transcripts, the protein bands for mERG1b were much weaker than those for mERG1a in our immunoblot analysis using an antibody that recognizes the common C-terminal epitope in both isoforms (Fig. 9). This might be attributable to differential accessibility of antibody to the common epitope in mERG1a and mERG1b (Jones et al. 2004). In mammalian heart, ERG1b protein expression has been clearly demonstrated using an isoform-specific antibody (Jones et al. 2004), whereas the antibodies against a common epitope recognized only ERG1a protein but failed to detect ERG1b (Pond et al. 2000). Further experiments are required to clarify the relative contribution of the mERG1b isoform to the generation of I_{Kr} in HL-1 cells.

Recently, siRNA has proven to be a powerful tool for investigating gene function by inducing knockdown phenotypes (Hannon 2002). In the present study, siRNA-mediated knockdown of mERG1 resulted in a dramatic decrease in I_{Kr}, providing direct evidence for an essential role of the mERG1 gene in the generation of I_{Kr} in HL-1 cells. It is possible to design siRNA for each isoform of mERG1 by targeting a specific exon sequence. Thus, our siRNA experiments suggested its potential application to the identification of gene products responsible for forming I_{Kr} in HL-1 cells. A major limitation of this approach was the difficulty of siRNA delivery into HL-1 cells. Our transfection efficiency using cationic lipids was <5%, which was sufficient for patch-clamp study but inadequate for biochemical analysis including measurements of mRNA and protein levels.

HL-1 Cells Are a More Reliable Source of I_{Kr} than AT-1 Cells

The electrophysiological characteristics of HL-1 cells seem to be qualitatively similar to those previously reported in their progenitor, AT-1 cells (Yang et al. 1994), except that the I_{Kr} density obtained from HL-1 cells in the present study (18 pA pF^{-1}) is three to four times larger than the value reported for AT-1 cells ($\sim$5 pA pF^{-1}) (Yang et al. 1994). Most importantly, they are quite different in their growth in culture. AT-1 cells proliferate to some extent in vitro, while extremely increasing their cell size, which is accompanied by changes in I_{Kr} density during primary culture (Yang et al. 1995). On the contrary, HL-1 cells can divide indefinitely in culture, while retaining their phenotype during continuous passages (Claycomb et al. 1998). In conclusion, taking advantage of their proliferative ability and stability of phenotype in culture, HL-1 cells can be adapted not only for electrophysiological experiments but also for biochemical and molecular biological experiments that require long-term culturing and provide a useful cardiac model for studies on the gating mechanisms, regulation by various signaling pathways, drug block and molecular basis of native I_{Kr} channels.

Acknowledgements This study was supported by a Grant-in Aid for Scientific Research from the Japan Society for the Promotion of Science. We are grateful to Dr. W. C. Claycomb for providing HL-1 cells.

References

Abbott GW, Sesti F, Splawski I et al (1999) MiRP1 forms I_{Kr} potassium channels with HERG and is associated with cardiac arrhythmia. Cell 97:175–187

Barajas-Martínez H, Elizalde A, Sánchez-Chapula JA (2000) Developmental differences in delayed rectifying outward current in feline ventricular myocytes. Am J Physiol 278:H484–H492

Carmeliet E (1992) Voltage- and time-dependent block of the delayed K^+ current in cardiac myocytes by dofetilide. J Pharmacol Exp Ther 262:809–817

Cavarra MS, del Mónaco SM, Assef YA et al (2007) HERG currents in native K562 leukemic cells. J Membr Biol 219:49–61

Chomczynski P, Sacchi N (1987) Single-step method of RNA isolation by acid guanidinium thiocyanate-phenol-chloroform extraction. Anal Biochem 162:156–159

Clark RB, Mangoni ME, Lueger A et al (2004) A rapidly activating delayed rectifier K^+ current regulates pacemaker activity in adult mouse sinoatrial node cells. Am J Physiol 286:H1757–H1766

Claycomb WC, Lanson NA Jr, Stallworth BS et al (1998) HL-1 cells: a cardiac muscle cell line that contracts and retains phenotypic characteristics of the adult cardiomyocyte. Proc Natl Acad Sci USA 95:2979–2984

Curran ME, Splawski I, Timothy KW et al (1995) A molecular basis for cardiac arrhythmia: *HERG* mutations cause long QT syndrome. Cell 80:795–803

Delcarpio JB, Lanson NA Jr, Field LJ et al (1991) Morphological characterization of cardiomyocytes isolated from a transplantable cardiac tumor derived from transgenic mouse atria (AT-1 cells). Circ Res 69:1591–1600

Field LJ (1988) Atrial natriuretic factor-SV40 T antigen transgenes produce tumors and cardiac arrhythmias in mice. Science 239:1029–1033

Hamill OP, Marty A, Neher E et al (1981) Improved patch-clamp techniques for high-resolution current recording from cells and cell-free membrane patches. Pflugers Arch 391:85–100

Hannon GJ (2002) RNA interference. Nature 418:244–251

Honjo H, Boyett MR, Kodama I et al (1996) Correlation between electrical activity and the size of rabbit sino-atrial node cells. J Physiol 496:795–808

Jones EM, Roti Roti EC, Wang J et al (2004) Cardiac I_{Kr} channels minimally comprise hERG 1a and 1b subunits. J Biol Chem 279:44690–44694

Lees-Miller JP, Kondo C, Wang L et al (1997) Electrophysiological characterization of an alternatively processed ERG K^+ channel in mouse and human hearts. Circ Res 81:719–726

Lei M, Honjo H, Kodama I et al (2001) Heterogeneous expression of the delayed-rectifier K^+ currents $i_{K,r}$ and $i_{K,s}$ in rabbit sinoatrial node cells. J Physiol 535:703–714

Liu DW, Antzelevitch C (1995) Characteristics of the delayed rectifier current (I_{Kr} and I_{Ks}) in canine ventricular epicardial, midmyocardial, and endocardial myocytes. A weaker I_{Ks} contributes to the longer action potential of the M cell. Circ Res 76:351–365

Liu Y, Taffet SM, Anumonwo JM et al (1994) Characterization of an E4031-sensitive potassium current in quiescent AT-1 cells. J Cardiovasc Electrophysiol 5:1017–1030

Liu S, Rasmusson RL, Campbell DL et al (1996) Activation and inactivation kinetics of an E-4031-sensitive current from single ferret atrial myocytes. Biophys J 70:2704–2715

London B, Trudeau MC, Newton KP et al (1997) Two isoforms of the mouse *ether-a-go-go*-related gene coassemble to form channels with properties similar to the rapidly activating component of the cardiac delayed rectifier K^+ current. Circ Res 81:870–878

Matsuura H, Ehara T, Ding WG et al (2002) Rapidly and slowly activating components of delayed rectifier K^+ current in guinea-pig sino-atrial node pacemaker cells. J Physiol 540:815–830

McDonald TV, Yu Z, Ming Z et al (1997) A minK-HERG complex regulates the cardiac potassium current I_{Kr}. Nature 388:289–292

McWhinney CD, Hansen C, Robishaw JD (2000) Alpha-1 adrenergic signaling in a cardiac murine atrial myocyte (HL-1) cell line. Mol Cell Biochem 214:111–119

Morais Cabral JH, Lee A, Cohen SL et al (1998) Crystal structure and functional analysis of the HERG potassium channel N-terminus: a eukaryotic PAS domain. Cell 95:649–655

Neilan CL, Kenyon E, Kovach MA et al (2000) An immortalized myocyte cell line, HL-1, expresses a functional δ-opioid receptor. J Mol Cell Cardiol 32:2187–2193

Niwa N, Yasui K, Opthof T et al (2004) $Ca_v3.2$ subunit underlies the functional T-type Ca^{2+} channel in murine hearts during the embryonic period. Am J Physiol 286:H2257–H2263

Ono K, Ito H (1995) Role of rapidly activating delayed rectifier K^+ current in sinoatrial node pacemaker activity. Am J Physiol 269:H453–H462

Phartiyal P, Jones EMC, Robertson GA (2007) Heteromeric assembly of human ether-à-go-go-related gene (hERG) 1a/1b channels occurs cotransfectionally via N-terminal interactions. J Biol Chem 282:9874–9882

Pond AL, Scheve BK, Benedict AT et al (2000) Expression of distinct ERG proteins in rat, mouse, and human heart. Relation to functional I_{Kr} channels. J Biol Chem 275:5997–6006

Roden DM, Lazzara R, Rosen M et al (1996) Multiple mechanisms in the long-QT syndrome. Current knowledge, gaps, and future directions. The SADS Foundation Task Force on LQTS. Circulation 94:1996–2012

Sale H, Wang J, O'Hara TJ et al (2008) Physiological properties of hERG 1a/1b heteromeric currents and a hERG 1b-specific mutation associated with long-QT syndrome. Circ Res 103: e81–e95

Sanguinetti MC, Jurkiewicz NK (1990) Two components of cardiac delayed rectifier K^+ current. Differential sensitivity to block by class III antiarrhythmic agents. J Gen Physiol 96:195–215

Sanguinetti MC, Jiang C, Curran ME et al (1995) A mechanistic link between an inherited and an acquired cardiac arrhythmia: *HERG* encodes the I_{Kr} potassium channel. Cell 81:299–307

Sartiani L, Bochet P, Cerbai E et al (2002) Functional expression of the hyperpolarization-activated, non-selective cation current I_f in immortalized HL-1 cardiomyocytes. J Physiol 545:81–92

Shibasaki T (1987) Conductance and kinetics of delayed rectifier potassium channels in nodal cells of the rabbit heart. J Physiol 387:227–250

Smith PL, Baukrowitz T, Yellen G (1996) The inward rectification mechanism of the HERG cardiac potassium channel. Nature 379:833–836

Trudeau MC, Warmke JW, Ganetzky B et al (1995) HERG, a human inward rectifier in the voltage-gated potassium channel family. Science 269:92–95

Wang L, Duff HJ (1996) Identification and characteristics of delayed rectifier K^+ current in fetal mouse ventricular myocytes. Am J Physiol 270:H2088–H2093

Wang L, Feng ZP, Kondo CS et al (1996) Developmental changes in the delayed rectifier K^+ channels in mouse heart. Circ Res 79:79–85

Weerapura M, Nattel S, Chartier D et al (2002) A comparison of currents carried by HERG, with and without coexpression of MiRP1, and the native rapid delayed rectifier current. Is MiRP1 the missing link? J Physiol 540:15–27

White SM, Constantin PE, Claycomb WC (2004) Cardiac physiology at the cellular level: use of cultured HL-1 cardiomyocytes for studies of cardiac muscle cell structure and function. Am J Physiol 286:H823–H829

Xia M, Salata JJ, Figueroa DJ et al (2004) Functional expression of L- and T-type Ca^{2+} channels in murine HL-1 cells. J Mol Cell Cardiol 36:111–119

Yang T, Roden DM (1996) Extracellular potassium modulation of drug block of I_{Kr}. Implications for torsade de pointes and reverse use-dependence. Circulation 93:407–411

Yang T, Wathen MS, Felipe A et al (1994) K^+ currents and K^+ channel mRNA in cultured atrial cardiac myocytes (AT-1 cells). Circ Res 75:870–878

Yang T, Kupershmidt S, Roden DM (1995) Anti-minK antisense decreases the amplitude of the rapidly activating cardiac delayed rectifier K^+ current. Circ Res 77:1246–1253

Yang T, Snyders DJ, Roden DM (1997) Rapid inactivation determines the rectification and $[K^+]_o$ dependence of the rapid component of the delayed rectifier K^+ current in cardiac cells. Circ Res 80:782–789

Yasui K, Liu W, Opthof T et al (2001) I_f current and spontaneous activity in mouse embryonic ventricular myocytes. Circ Res 88:536–542

Zankov DP, Yoshida H, Tsuji K et al (2009) Adrenergic regulation of the rapid component of delayed rectifier K^+ current: implications for arrhythmogenesis in LQT2 patients. Heart Rhythm 6:1038–1046

Zhou Z, Gong Q, Ye B et al (1998) Properties of HERG channels stably expressed in HEK 293 cells studied at physiological temperature. Biophys J 74:230–241